Small but Mighty: Incorporating Fe_3O_4 Nanoparticles into PES Membranes for Enhanced Water Treatment Efficiency

Gandomkar, Elahe•; Fazlali, Alireza*+

Department of Chemical Engineering, Faculty of Engineering, Arak University, Arak, I.R. IRAN

ABSTRACT: *This study focused on developing a new membrane type by incorporating magnetic iron oxide nanoparticles (Fe_3O_4) into a polyethersulfone (PES) matrix to create a Fe_3O_4/PES membrane. The synthesized membrane was characterized using various techniques, including SEM, Map, 3D images, TEM, XRD, and FT-IR, to determine its structure and properties. The membrane's performance was evaluated by examining parameters such as water contact angle, membrane pore size and porosity, water content, Pure Water Flux (PWF), and salt rejection. The results showed that the Fe_3O_4/PES membrane outperformed the pure PES membrane regarding water flux and salt rejection. The membrane with a Fe_3O_4 concentration of 0.01wt.% had the highest flux value of 16.35 (L/m^2h), while the virgin membrane's flux value was only 2.81 (L/m^2h). Furthermore, the salt rejection of the modified membrane increased from 60% to 90% compared to the pure PES membrane. It was observed that the Fe_3O_4 nanoparticles, which had a positive charge of 3-7 nm, tended to agglomerate and increase in size when the Fe_3O_4 concentration was increased, leading to a negative surface charge. By using fewer Fe_3O_4 nanoparticles, the Fe_3O_4/PES membrane achieved similar performance as other research, making it a more cost-effective option.*

KEYWORDS: *Magnetic iron oxide nanoparticles; Polyethersulfone (PES) matrix; Fe_3O_4/PES membrane; Membrane characterization; Surface charge; Cost-effective option.*

INTRODUCTION

The production of Nano Filtration (NF) membranes with specific properties, such as high rejection, antifouling ability, and water flux, is a critical stage in water treatment and purification. The shape and surface chemistry of NF membranes is practically significant due to their connection to separation effectiveness and antifouling behavior. Membrane fouling is a severe issue that affects membrane selectivity, lifespan, and flow. In general, membranes with hydrophilic surfaces have remarkable antifouling qualities. The hydrophilicity and antifouling capacity of NF membranes have been improved through numerous approaches, including surface grafting, coating,

**To whom correspondence should be addressed.*

+ E-mail: A-Fazlali@araku.ac.ir

• Other Address: District No.1, Arak Education Department, Education Department of Markazi Province, Ministry of Education, Arak, I.R. IRAN.

1021-9986/2023/10/3449-3466 18/$/6.08

polymer mixing, and introducing polymer matrix with hydrophilic NanoParticles (NPs) [1-3]. The simplest and most common method is thought to be the integration of hydrophilic nanoparticles into the membrane body [4, 5].

It is known that metallic oxide nanoparticles, such as TiO_2, SiO_2, and Fe_3O_4, are employed to alter NF membranes. The majority of responders claimed that changed membranes showed noticeable performance changes. Fe_3O_4 is a hydrophilic and chemically stable magnetic nanoparticle due to the surface hydroxyl groups. These inexpensive materials have excellent reactivity, ion exchange capacity, adsorption capacity, and environmental safety. However, they cannot be dissolved in organic solvents, and proper dispersion is achieved in a suitable solution. Numerous studies have been done to prevent the aggregation of nanoparticles from attaining high efficiency.

Three categories can be made for magnetic nanoparticle modification techniques: covering the surface of NPs with an adsorptive layer, immobilizing a reactive ligand, and combining upper items. Furthermore, modifying the surface of NPs might improve their affinity for membrane structures. Polyvinylpyrrolidone (PVP) is a great option for NP modification because of its capacity to create covalent connections with the surfaces of magnetic nanoparticles. Additionally, PVP is a non-toxic, inert polymer[6-11]. It is an amphiphilic polymer because of the pyrrolidone and alkyl groups present in its structure, making it both hydrophilic and hydrophobic[5, 12-18].

Fe_3O_4 is a hydrophilic and chemically stable magnetic nanoparticle due to the surface hydroxyl groups. This material is inexpensive and has excellent reactivity, ion exchange capacity, adsorption capacity, and environmental safety. Rejection rates for NaCl and $MgSO_4$ were reported to be 68 and 82 percent, respectively, when Fe_3O_4 nanoparticles were added to a PES matrix.[19] Numerous surface modifications have been studied since interactions between nanoparticles and polymers heavily depend on the latter's surface.[20-22] The impact of Congo red dye adsorption-based removal using magnetite nanoparticles (Fe_3O_4) coated with polyvinyl pyrrolidone (PVP) was studied.[19] The effects of functionalized (amine and metformin) and modified (immobilizing silica-Fe_3O_4 NPs) iron oxide NPs have been examined on the segregation performance of PES-based nanofiltration membranes. Due to their improved hydrophilicity, porosity, and mean pore radius, nanocomposite membranes showed a significant pure water flux. Copper ion elimination is likely due to the nucleophilic functional groups and the hydrophilic surfaces of nanocomposite membranes. Separately, PES-based NF membranes incorporating carboxymethyl chitosan- Fe_3O_4 (FRR) showed high water flow and flux recovery ratios.[7, 20, 23, 24]

Numerous surface modifications have been studied to understand the interactions between nanoparticles and polymers, as these interactions heavily depend on the surface properties of the latter [7, 21, 22]. One study examined the impact of using magnetite nanoparticles (Fe_3O_4) coated with polyvinyl pyrrolidone (PVP) for the removal of Congo red dye [19]. Other studies investigated the effects of using functionalized (amine and metformin) and modified (immobilizing silica- Fe_3O_4 NPs) iron oxide NPs on the segregation performance of PES-based nanofiltration membranes. Nanocomposite membranes, with improved hydrophilicity, porosity, and mean pore radius, demonstrated a significant pure water flux. Copper ion elimination was likely due to the nanocomposite membranes' nucleophilic functional groups and hydrophilic surfaces. Additionally, PES-based NF membranes incorporating carboxymethyl chitosan- Fe_3O_4 (FRR) showed high water flow and flux recovery ratios [7, 21, 25].

Incorporating PANI and MWCNT (iron oxide) nanoparticles onto PES-based NF membranes produced considerable Cu antifouling characteristics and rejection against proteins [20]. Another study used Fe_3O_4@SiO_2@MPS@poly(4-vinyl pyridine) NPs to remove nitrate from water. Fe_3O_4 nanoparticles were also used to functionalize hollow fiber polyetherimide membranes on their surface. The modified membranes showed notable hydrodynamic permeability and antifouling properties against the development of bacteria and proteins [26].

Modifying the surface of NPs can improve their affinity for membrane structures. Particle size and shape heavily influence nanomaterials' surface potential, surface characteristics, and chemical properties. Iron oxide surfaces have become popular at the nanoscale due to their increased surface properties [27, 28]. Using nanoparticles with smaller sizes than their common and commercial is recommended because surface properties increase with size reduction, and each material's characteristic properties change tremendously with size reduction. For instance,

Table 1: The details of composition for the preparation of Fe_3O_4/ PES membranes

Membrane Sample	PES (wt. %)	PVP (wt. %)	Fe_3O_4 (wt. %)	DMAc (wt. %)
SF_0	18	1	0	81.00
SF_1	18	1	0.01	80.99
SF_2	18	1	0.03	80.97
SF_3	18	1	0.1	80.90
SF_4	18	1	0.3	80.70
SF_5	18	1	0.5	80.50

the characteristic property of gold nanoparticles is color change with size reduction in the nano range. As the size of iron nanoparticles reduces, their active surface area and interaction with polymers increase. The nanoparticles' dispersity is predicted to increase with the polymer solution substrate. A membrane with acceptable properties can be obtained by consuming a smaller amount of nanoparticles.

Although iron oxide surfaces are essential in establishing a material's characteristics, research on the properties of iron nanoparticles at the smallest sizes has not yet been conducted, as synthesizing iron nanoparticles at this scale is challenging, and their magnetic characteristics become stronger as their size decreases [29-31]. Recent research has started to produce atomistic simulations of these surfaces. This study investigated the effects of blending hydrophilic super magnetic (Fe_3O_4) nanoparticles with PES-based NF membranes for their physicochemical characteristics, separation effectiveness, and antifouling capability. The effect of Fe_3O_4 nanoparticles on the PES membrane matrix and the alteration of PES-based nanofiltration membrane characteristics by Fe_3O_4 nanoparticles has not been studied. No information is available in the literature. The shape of membranes was investigated using scanning electron microscopy (SEM) and three-dimensional pictures. The impact of nanoparticle integration on membrane properties and performance was further examined using water contact angle, water content, membrane pore size and porosity, FT-IR, XRD, water flux, and salt rejection.

EXPERIMENTAL SECTION

Materials and reagents

$FeCl_3.6H_2O$, $FeCl_2.4H_2O$, ethanol (98%), NH_4OH, polyvinylpyrrolidone (PVP, M_w = 25000 g/mol) and *N, N*-Dimethylacetamide (DMAc, M = 87.12 g/mol) provided by Merck Inc and Polyethersulfone (PES) (Ultrason E6020P, M_w: 58000) was supplied by BASF Co. (New Jersey, USA) were used.

Preparation of Fe_3O_4 nanoparticles

A solution of NH_4OH 25wt% was added dropwise (1 mL/min) to a mixture of 5.16 g of $FeCl_2$ and 14.16 g of $FeCl_3$ while stirring the mixture at 80˚C until the pH reached 10. Ethanol was added to the mixture to stop the reaction. Then, the NPs were separated with a magnet and the pH was restored to neutral. The obtained magnetic NPs were washed with ethanol and deionized water several times and then dried at 60˚C under vacuum for 11 hours. Magnetic NPs were synthesized in two ways: the first experiment was performed under atmospheric conditions, and the second under N_2 gas [30-33].

Preparation of PES-based nanofiltration membranes

The phase inversion method was used to prepare the NF membrane [34, 35]. In brief, PES (18 wt.%) and PVP (1 wt.%) were dissolved in DMAc and stirred for 7h. Different amounts of Fe_3O_4 NPs (0, 0.01, 0.03, 0.05, 0.1, 0.3, and 0.5 wt.%) were added to the polymeric solutions and sonicated for 30 minutes using an ultrasonic bath (Parsonic 11S model, S/N PN-88159, Iran). The obtained solution was left at ambient temperature to remove air bubbles. Subsequently, the polymeric solution was cast on clean glass plates at room temperature using a film applicator with a thickness of 150 µm. The resulting films were immediately immersed in DI water. The prepared Fe_3O_4/PES membranes were then stored in DI water [36, 37]. The details of the composition for preparing Fe_3O_4/PES membranes are provided in Table 1.

Characterization

Morphological studies

Different tests were conducted to characterize the final product, including SEM, EDX Mapping, XRD, Particle

Table 2: Condition of synthesis of NPs and their average diameter sizes

Sample	Fe^{2+}/ Fe^{3+}	HCl (mL)	Base	Synthesized Atmosphere	Synthesized Condition	Diameter (nm)
1	2	-	NH_3	Ambient Air	Stirring-Coprecipitation	7.1
2	2	-	NH_3	N_2	Stirring-Coprecipitation	3.7*

* Selected particles for membrane modification

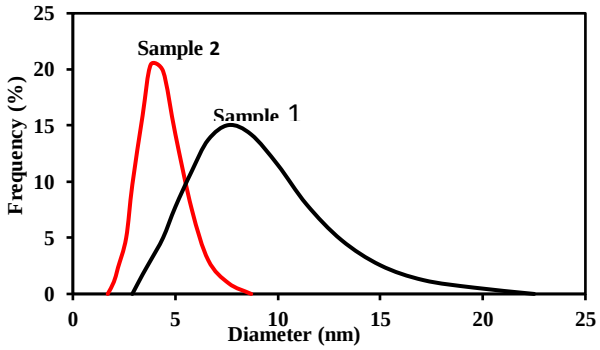

Fig. 1: PSA image of Samples 1 and 2

Size Analysis (PSA), FT-IR and TEM. FESEM (Holland Philips XL30 microscope) was used to characterize the size and morphology of the Fe_3O_4 NPs. Moreover, FESEM (TESCAN, MIRA III, and the Czech Republic) was utilized to characterize membranes' surface and cross-section morphology and mapping. A particle size analyzer (LB-550 Horiba, Japan) was used to find the nanostructure's size distribution. The crystalline phase of different particles was examined by X-ray diffraction (Holland Philips X-ray diffractometer with Cu-Kα radiation, λ = 1.54178 Å). Furthermore, the 3D surface images and Mountains (R) software (version 6.4) were used to study the prepared membranes' surface morphology.

Membrane water contact angle, water content, porosity and mean-pore size

A contact angle analyzer (Data physics-OCA15 PLUS) was used to determine the water contact angle and membrane hydrophilicity. Four different locations were considered to minimize experimental errors.

In Eq. (1), differences between dry and wet membrane weights were used to determine the amount of membrane water content. For this purpose, membranes dried in an oven at 60 ˚C [36, 38, 39]:

$$\text{Water content} = (W_w - W_d)/W_w \times 100 \quad (1)$$

Eq. (2) was used to calculate the porosity (ε) of the fabricated membranes [7, 39]:

$$\varepsilon(\%) = (W_w - W_d)/\rho V_m \times 100 \quad (2)$$

Eq. (3), the Guerout-Elford-Ferry Equation, was used to calculate mean pore size (r_m) for all membranes [39, 40]:

$$r_m = \sqrt{((2.9 - 1.75\varepsilon)8\eta LQ/\varepsilon A\Delta p)} \quad (3)$$

where W_d, W_w, V_m, ρ, η, L, Q, A, Δp, and ε are dry and wet weight (g), membrane volume (cm^3), water density (g/cm^3), the water viscosity (8.9×10^{-4} Pa.s), the membrane thickness (m), the volume of the permeated WF (m^3/s), the membrane filtration area (m^2), operating pressure (0.45MPa), and membrane porosity, respectively.

Membrane Separation Performance

A homemade dead-end filtration system performed the filtration test. The effective area of the treatment system was 11.94 (cm^2). Membrane compaction was performed in 5 bars before the filtration test by deionized water. Equation (4) was applied to the PWF of NF membranes [25, 39]:

$$J = V/At \quad (4)$$

Equation (5) was utilized to calculate the salt rejection ability

$$R(\%) = (C_f - WC_p)/C_f \times 100 \quad (5)$$

Where V, A, Δt, J, C_f, and C_p are the volume of permeate flux (L), membrane area (m^2), testing time (h), permeation flux (L/m^2h), the salt concentration in the feed and salt concentration in permeate, respectively [41-43]. All experiments were done at 25˚C. Na_2SO_4 solution (1g/L) was considered to evaluate the salt elimination ability of NF membranes.

RESULTS AND DISCUSSION

Characterization of Fe_3O_4 nanoparticles and Fe_3O_4/PES membrane

Fig. 1 shows particle size analysis of samples under different reaction conditions. The results are presented in Table 2. The results of PSA show that the particle size decreased when the reaction was performed under N_2 gas.

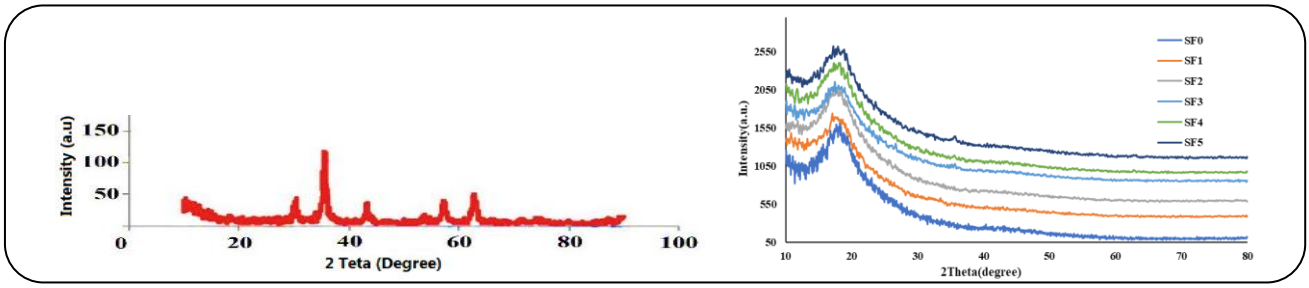

(a) *(b)*

Fig. 2: XRD pattern (in arbitrary units) of a) Fe_3O_4 NPs and b) SF0, SF1, SF3 and SF6

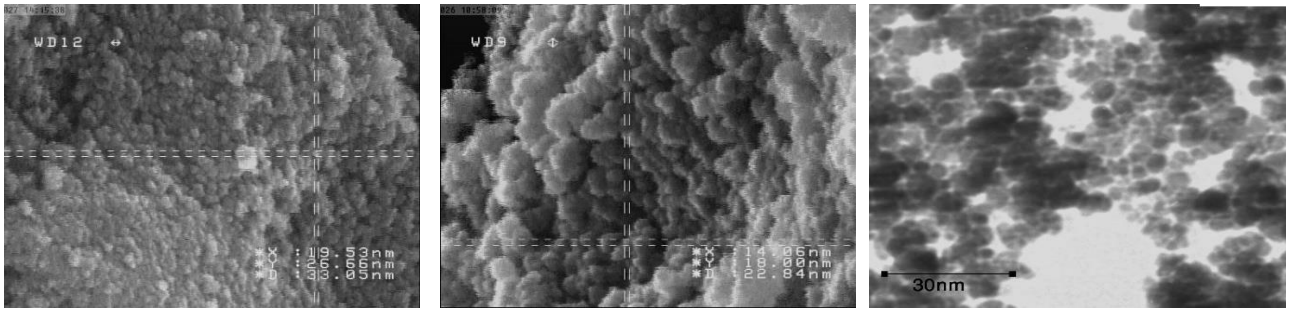

(a) *(b)* *(c)*

Fig. 3: SEM images of a) Sample 1 and b) Sample 2 and c) TEM Image of Sample 2

The XRD pattern (Fig. 2a) shows the crystal structure of the Fe_3O_4 NPs. The sharp peaks of the XRD pattern are related to the synthesized Fe_3O_4 NPs. Some sharp Bragg reflections could be indexed as the Face-Centered Cubic (FCC) structure of Fe_3O_4 with the corresponding diffraction peaks of (111), (220), (311),(400), (422), (511), (440), and (533) planes [44-46]. The reflection peaks appear broader, indicating synthesized Fe_3O_4 NPs with small sizes. The XRD pattern of Fe_3O_4 agrees with the JCPDS card No. 19-0629, having the characteristic peaks at 2θ: 35, 36, 43, 57, and 62. No impurity was observed [44-46]. The fitted image shows no other diffraction peak in the sample, which confirms the pure crystalline phase of the synthesized Fe_3O_4. According to the Scherrer equation, the average crystal size of the Fe_3O_4 NPs was 3.7 nm.

Fig. 2b shows one prominent peak at 2θ =26- 28°, similar to the reported peak for pure PES [47]. For the Fe_3O_4/PES membranes, some new peaks at 2θ = 12, 35, 36°, and 43° were observed. These peaks are characteristic of iron oxide, which confirms the presence of Fe_3O_4 NPs in the PES membrane. These XRD patterns show that the Fe_3O_4 NPs have been distributed into the polymer body, and the nano-enhanced membranes remained amorphous with the incorporation of NPs into PES.

The morphologies of Fe_3O_4 NPs were determined *via* SEM and TEM. Fig. 3a and Fig.3b show SEM images of Fe_3O_4 NPs prepared by the co-precipitation method under different conditions. Fig. 3c shows the TEM image of Fe_3O_4 NPs synthesized under N_2 gas. According to Fig.3c, it is evident that the Fe_3O_4 NPs have narrow distribution sizes and regular spherical particle shapes with an average size of 3nm. The difference between samples 1 and 2 is evident in Figs 3a and 3b, respectively. The particle size is more extensive in Fig.3a. In Fig.3b, the particles are stacked in sharper cones due to the more potent magnetic force to reduce the surface potential further.

FT-IR analysis presented in Fig. 4a shows peaks near 660 cm^{-1} and 594 cm^{-1}, which can be assigned to Fe-O stretching[48]. The broad peaks around 1630 cm^{-1} and 3440 cm^{-1} can be ascribed to the O-H stretching modes and bending vibration. Specific absorption peaks can be identified for pure PES membranes. Composite membranes in Fig. 4b show that the S=O stretching peaks were present at 1170 cm^{-1} and 1108 cm^{-1}. The hydrogen bond O-H stretching modes and bending vibration stretching peaks became broad in the 3000 cm^{-1} - 3700 cm^{-1} regions. The peak of the CO stretching was observed at 1073 cm^{-1}. The C-H stretching peak of the benzene ring in the PES structure was located at 3097 cm^{-1}. The C-O-C stretching

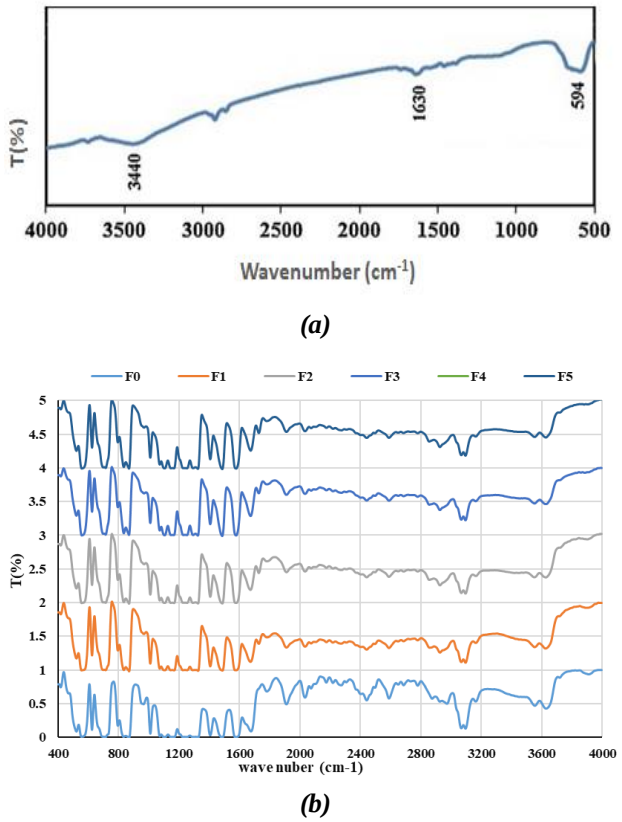

Fig. 4: FT-IR pattern a) Fe_3O_4, b) PES (SF0) and Fe_3O_4/PES membranes (SF1 to SF5)

peaks were situated at 1329 cm^{-1} and 1226 cm^{-1}. Three peaks between 1600 cm^{-1} and 1400 cm^{-1} were attributed to aromatic skeletal vibration. However, because of the presence of firm peaks of PES absorption bands, Fe-O stretching peaks were not observed in intensity. They are shown in Fig 4b in red lines for comparing pure PES and blended membranes. These red lines indicated characteristic peaks in the bonds between S, O, and C atoms of PES and Fe_3O_4 atoms.

The morphological changes and dispersion at different concentrations of Fe_3O_4 NPs were investigated by FESEM cross-sectional images. As shown in Fig 5, all specimens have an asymmetric structure with a dense upper layer and a porous sub-layer. The exchange rate between non-solvent and solvent can be affected by incorporating hydrophilic Fe_3O_4 NPs into the polymer solution [49, 50]. Faster solvent removal leads to the active layer's rapid formation, which causes excessive resistance to mass transfer and increases the required time for the exchange of solvent and non-solvent under the layer. Thus, the cavities in the substrate of the sponge-like structure become a finger structure [51-53]. FESEM images showed that the increase in Fe_3O_4 NPs in the membrane structure resulted in a significant increase in the size of finger-like channels in the substrate of the modified membranes compared to the pure PES membrane [39, 54, 55]. The presence of Fe_3O_4 as a hydrophilic additive with similar non-solvent (water) properties in the polymer solution leads to further insolubility of polymers due to the formation of iron oxide-polymer bonds, which reduces the interaction of polymer chains. It ultimately leads to faster phase inversion of the polymer solution in the non-solvent. As a result, this type of behavior leads to the formation of larger cavities in the membrane structure [47].

Thus, due to Fe_3O_4 NPs hydrophilicity, phase inversion occurred more rapidly, creating membrane cavities with a finger-like structure. The cavities and channels are irregular, the active layer is thick and the channels stretched to the end are very wide. From samples SF1 onwards, the thickness of the active layer has increased, especially in samples SF3, SF4, and SF5. Moreover, the beginning of the channels is not close to the surface of the membrane. On the other hand, the blockage of cavities and channels has occurred with NPs.

FESEM images of the membrane surface (Fig. 6) confirm the good dispersion of Fe_3O_4 NPs in samples SF1 and SF2 and also confirm the formation of lumps on samples SF3 and later.

The cross-sectional analysis mapping for element Fe is shown in Fig 7 for SF1 and SF3. As shown in Fig 7, the diffusion of the Fe element in the membranes is good in both samples. Although it is evident in Fig 7b, the image shows a few hunks of Fe_3O_4 NPs inside the membrane.

3D surface images were used to study the membrane surface morphology (Fig 8). According to Table 3, the average surface roughness obtained for SF0 was 17.6 nm, which increases with the combination of Fe_3O_4 NPs for SF1 and SF2. Increased surface roughness due to improved membrane heterogeneity results from the presence of NPs in the membrane body. The hydrophilic properties and low density of Fe_3O_4 NPs place them on the surface of the membrane. For SF4 and SF5, it has been observed that Ra is reduced, and the membrane surface is softer. The higher content of NPs can cause scratches due to reducing the distance between the NPs in the casting solution.

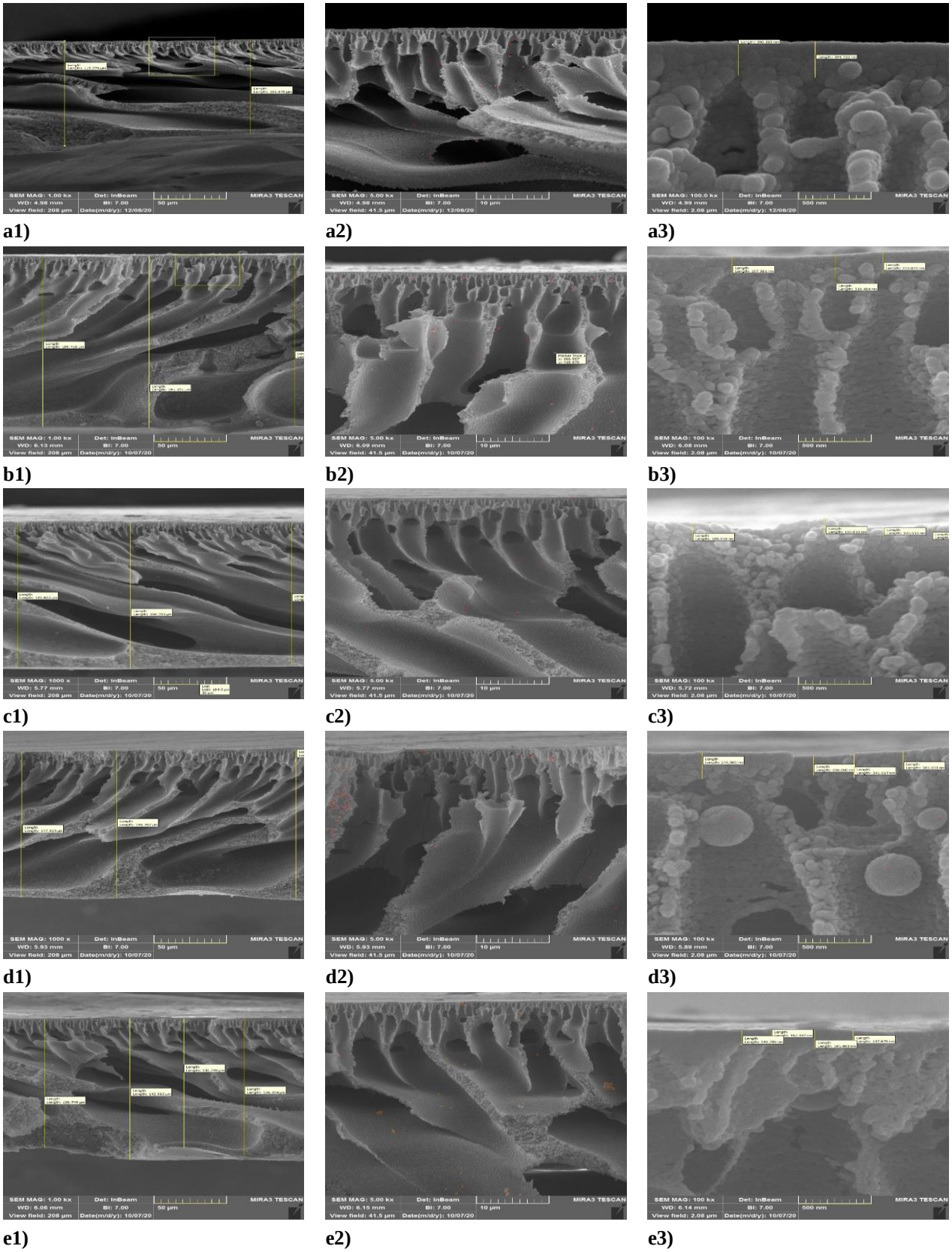

a1) **a2)** **a3)**

b1) **b2)** **b3)**

c1) **c2)** **c3)**

d1) **d2)** **d3)**

e1) **e2)** **e3)**

Fig. 5: The cross-sectional SEM images of a)SF1, b)SF2, c)SF3, d)SF4 and e)SF5

Table 3: The Surface roughness parameters of Fe_3O_4/PES membranes

	SF0	SF1	SF2	SF3	SF4	SF5
Roughness average (Ra) (nm)	2.18	4.011	3.04	3.77	4.67	4.64
Root mean square roughness (Rq) (nm)	2.85	5.48	3.39	4.94	6.05	7.45
Mean Ht (nm)	12.70	19.42	24.91	24.32	24.36	30.15
Median Ht (nm)	12.90	19.04	24.87	24.41	24.37	29.91

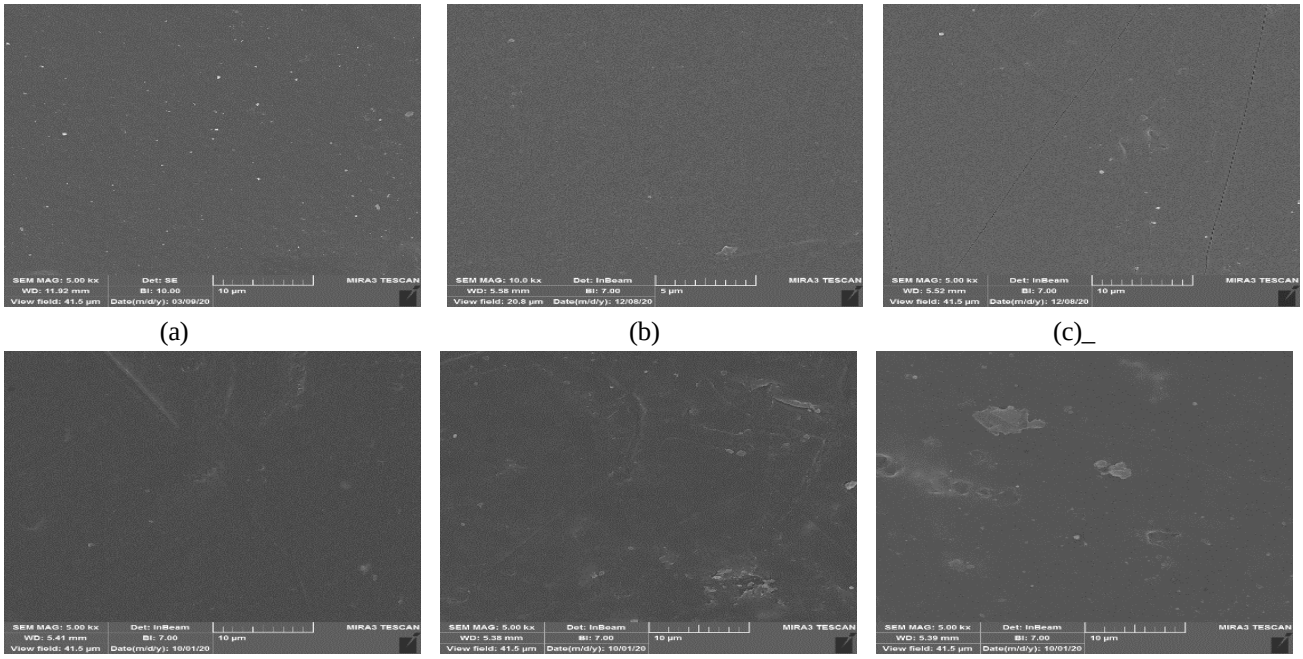

(a) (b) (c)_

(d) (e) (f)

Fig. 6: SEM Surface images of a)SF0, b)SF1, c)SF2, d)SF3, e)SF4 and f)SF5

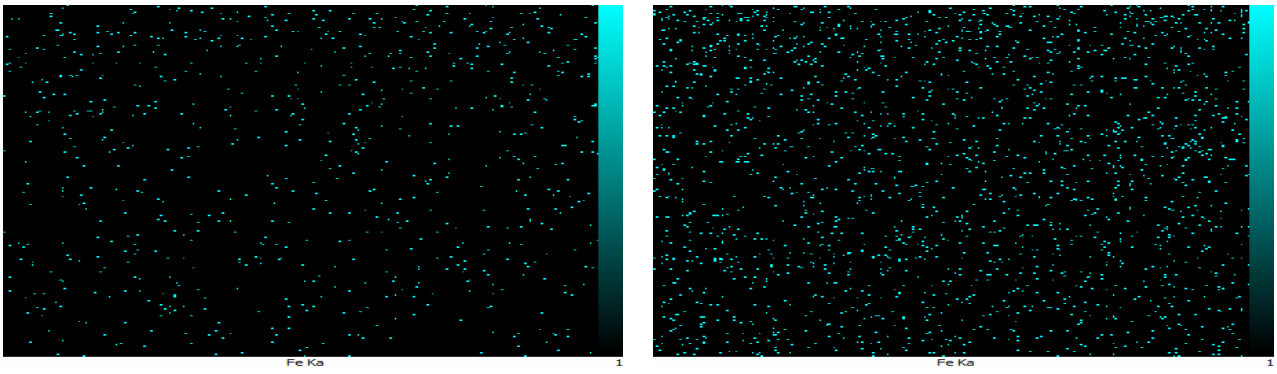

(a) **(b)**

Fig. 7: EDX mapping of (Fe) for a)SF1 and b)SF3

Moreover, the viscosity of the casting solution increases with the increasing amount of NPs [56, 57]. Increasing the casting solution viscosity can decrease the rate of the phase inversion process [56, 58, 59], and due to the delay in mixing, the NPs will clump together. However, at high concentrations of NPs (SF5) the surface roughness increases again due to the release of enormous masses of magnetic NPs by the weight of hunks and the stirrer magnetic field. The membrane surface roughness and heterogeneity are mainly due to the agglomeration

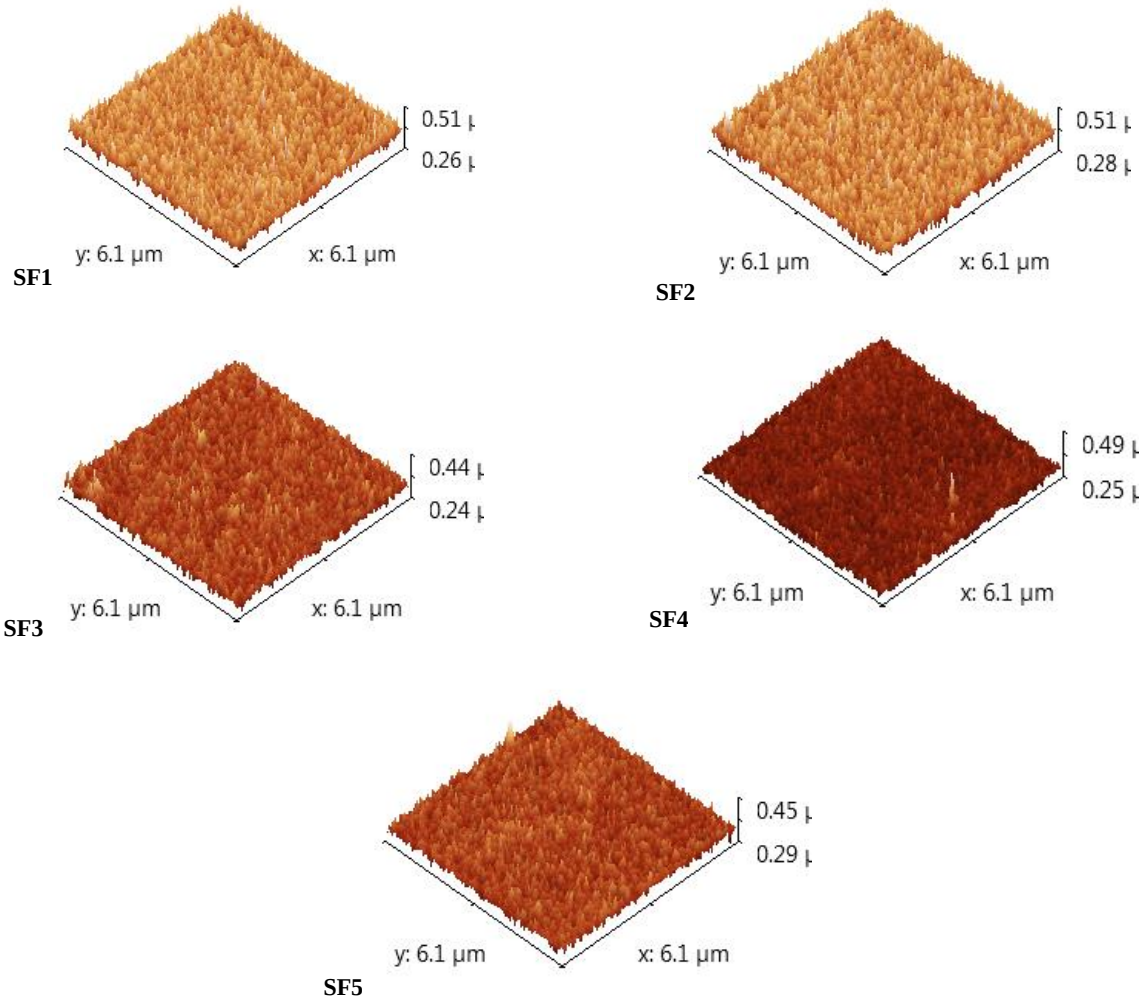

Fig. 8.: The 3D surface images of the Fe_3O_4/ PES membranes SF1 to SF5 and

of NPs in high concentrations. In addition, Rq, which indicates the effect of roughness caused by valleys and peaks, increases with increasing nanoparticle concentration. In SF1, the increasing concentration of NPs resulted in rising average roughness. However, in sample SF2, average roughness decreased sharply, showing the agglomeration's effect. In samples SF2 to SF4, agglomeration increases the roughness, but in sample SF5, it reduces slightly. An increase in the average height of the roughness indicates that the clumps became bulky regionally.

Water contact angle and hydrophilicity

The contact angle is essential in membrane investigation as it indicates the wetting and the hydrophilicity behavior. A hydrophilic membrane is useful as it shows low fouling and high water flux properties.[60] According to literature reports, a membrane's PWF, pore size, and porosity affect its contact angle.[61-66] A membrane's porosity and pore size significantly affect its contact angle more than PWF.[67] Research on hydrophilicity suggests that hydrophilicity depends on two general chemical and physical factors. The chemical factor depends on the functional groups, chemical bonds, and the resulting surface energy. The physical factor depends on the surface roughness, the work function, peak height and width. Contact angle measurements for PES membranes embedded with Fe_3O_4 are shown in Fig 9. The addition of Fe_3O_4 NPs is expected to reduce the contact angle and, as a result, increase hydrophilicity. However, the results show that the membrane contact angle did not change significantly after embedding the hydrophilic Fe_3O_4 NPs.

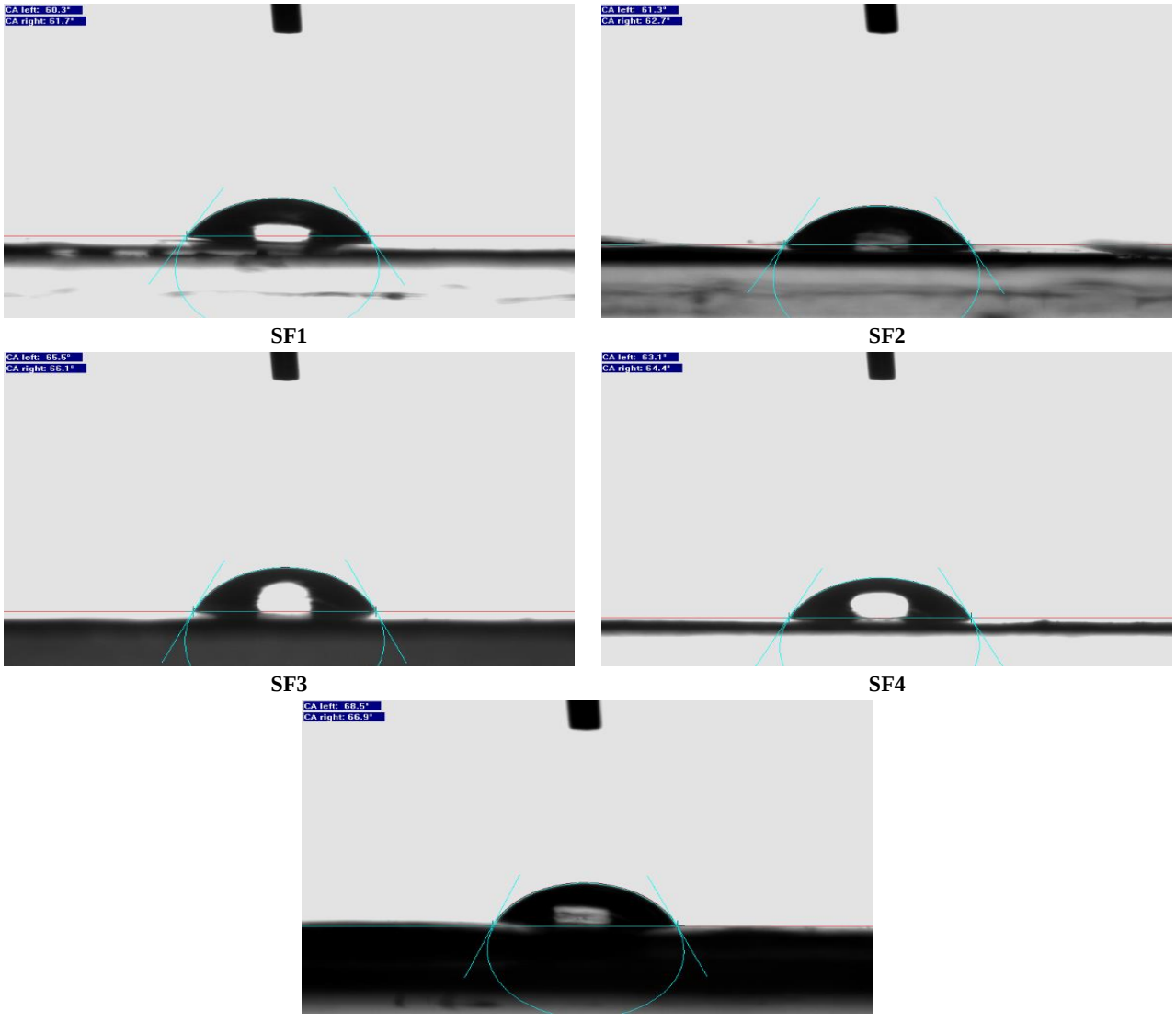

Fig. 9: The water contact angle of all fabricated membranes

It may be concluded that the NPs are coated with PES but are not in direct contact with water droplets. However, it should be noted that the contact angle between a surface and a drop of water depends not only on the surface chemistry but also on the super magnetic properties, the surface roughness, and the very high surface charge of ultra-fine Fe_3O_4 NPs. Evidence shows that combining Fe_3O_4 NPs in polymer membranes increases the membrane's roughness, especially in mineral NPs. According to Wenzel's model, the degree of roughness should be such as to enhance the wettability of the surface relative to its inherent tendency to roll or form a film of liquid. It means that roughness can reduce the contact angle for a surface such as a PES with a contact angle of fewer than 90 degrees. On the other hand, hydrophilic Fe_3O_4 NPs composition is expected to reduce hydrophilicity and contact angle.

However, tiny Fe_3O_4 NPs stick together to reduce the surface energy and form larger masses as the nanoparticle concentration increases (SF4). Therefore, the active surface area of the NPs is reduced, thus reducing the chemical properties and functional groups that can be formed on the surface.

In SF1, due to the surface charge, a strong hydrogen bond is created and the surface chemistry and chemical parameters, despite the high roughness, increase the hydrophilicity compared to other samples. Its low angle is due to the positive effect of chemical parameters, surface

Table 4: The Water contact angle amounts for the Fe_3O_4 /PES membranes

Membrane No.	Contact angle (°)	Fe_3O_4 (wt. %)
SF1	61	0.01
SF2	62	0.03
SF3	65.8	0.1
SF4	63.9	0.3
SF5	67.7	0.5

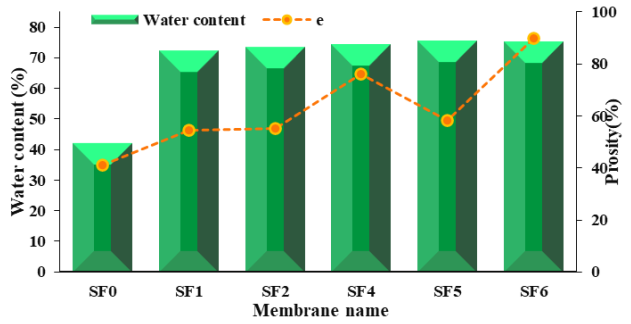

Fig. 10: The water content and the porosity of all fabricated membranes

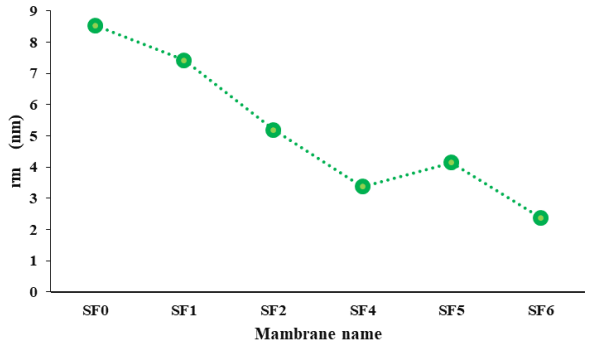

Fig. 11: The calculated mean pore size of the Fe_3O_4 /PES membranes

chemistry and magnetic properties in reducing the contact angle, thus increasing the hydrophilicity consistent with Wenzel's model. In membranes SF2 and SF3, although the roughness has decreased compared to SF1, the height of the average roughness and the geometric average of the roughness have increased due to the agglomeration. Also, its chemical and magnetic parameters have decreased, resulting in almost zero surface charge. The roughness height causes some air to get stuck in these valleys caused by the roughness and according to the Cassie-Baxter model, the visual contact angle increases. In sample SF4, the contact angle is expected to increase with increasing roughness, as in samples SF2 and SF3. However, it is observed that the contact angle decreases due to the increasing size of iron NPs, and the surface charge of iron becomes negative. It increases the strength of surface chemical parameters, which by reducing the angle, Wenzel's model prevails in these conditions. And in the last sample, it is like 5, with the difference that with increasing the volume of agglomeration, the charge ratio to the effective surface of the agglomerated NPs decreases. On the other hand, the roughness height rises slightly, and these two factors slightly increase the contact angle and hydrophilicity. Various factors affect the roughness; increasing the roughness and height have a negative effect, chemical and hydrophilic characteristics have a positive impact, and the surface chemistry concerning the structure should be investigated.

Membrane water content

According to Fig. 10, the modified membrane's water content increases compared to the virgin PES membrane. Because hydrophilic Fe_3O_4 NPs increase the hydrophilicity of membranes [68]. Fig. 10 shows that the blended membrane's water content and porosity increase with increasing Fe_3O_4 NPs, due to the hydrogen bond between Fe_3O_4 NPs and water molecules. So, improving the phase inversion process and forming larger and longer void spaces at higher concentrations of Fe_3O_4 NPs (SF3, SF4, and SF5 samples) shows that it can reduce the membrane's ability to retain water, porosity, and water content. This can be due to the accumulation of NPs and reduced active sites of iron oxide. Therefore, it causes the reduction of hydrogen bonds and closes the channels, thus reducing water transfer through the membrane pores. The nanoparticles' intermolecular forces and the polymer and water may disrupt the membrane structure during phase inversion.

In contrast, at the entrance to the blocked channels, the channels may be connected at a shorter distance from the thin layer to form a larger space so that porosity can be increased (SF5, Fig. 5). In addition, Fig. 11 shows the average pore size of the prepared membranes increases

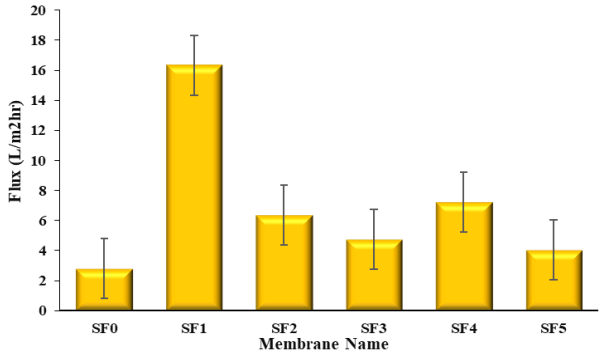

Fig. 12: The flux of the prepared membrane (SF0 to SF6)

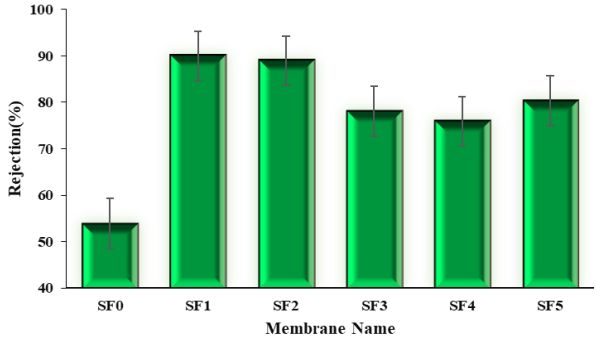

Fig. 13: Salt rejection percent in modified membrane

with increasing the concentration of NPs. However, by the strong magnetic interaction of tiny Fe_3O_4 NPs, the accumulation of NPs on the surface and inside the membrane can play an essential role in the hole size of the membrane structure. Under these conditions, the transport channels can be blocked, and thus, the flux is reduced. No acceptable flux was observed from the SF3 sample onwards [69].

Membrane separation performance

Membrane hydrophilicity and membrane morphology are two parameters that affect the amount of flux, and flux increases with the improvement of these two parameters. The presence of Fe_3O_4 NPs as hydrophilic NPs increases the membrane's hydrophilicity and leads to increased water flow through the membrane. Besides, membrane morphology and structure characteristics affect flux, such as increased porosity, increased mean pore size, reduced high-density layer thickness, and improved membrane channel shape. According to the results, using hydrophilic Fe_3O_4 NPs in the membrane structure increases water penetration into the polymer film. Also, it increases the rate of solvent penetration from the membrane into the water during the phase inversion process. Therefore, empty spaces and cavities are vast in the membrane structure, which improves the flux. On the other hand, as shown in Fig. 9, as the amount of Fe_3O_4 NPs increases, the water contact angle decreases, which indicates an improvement in hydrophilicity and flux (Fig. 12). The rise in flux for SF1 16.35 (L/m^2h) and SF5 7.25 (L/m^2h) is very significant compared with SF0 as the neat PES membrane 2.81 (L/m^2h).

By increasing the concentration of NPs from sample SF3 onwards, the flux so much decreased that its data as NF membrane flux were not acceptable, so its data were not reported. As the polymer solution's viscosity increases and the phase inversion rate decreases (Fig.5), the increase in the top layer's thickness also acts as a layer of resistance to water molecules' transfer. In addition, the tendency of NPs to accumulate causes blockage of membrane cavities, which reduces porosity and pore size[70, 71]. Note that despite the decrease in flux at higher concentrations reported of Fe_3O_4 NPs, the flux obtained for the modified membranes is more than a neat membrane, which indicates the favorable effects of Fe_3O_4 NPs on flux. Comparing Fig. 12 and Fig. 11, it is clear that the studied membranes' flux behavior is almost similar to the mean pore size diagram's action. This study has three general separation mechanisms: chemical-magnetic, sieving, and Donan electrostatic. The dominant mechanism is determined according to Fig. 13 and considering other analyses (especially Fig. 4b). Since in sample SF1, Fe_3O_4 NPs are very well dispersed and no lumps are observed. The effective size of NPs is tiny, so they have a very high electrostatic force per unit area, and active sites are much stronger than other samples. It can be seen that the chemical bonds and electrostatic force of Donan positively affect this separation.

On the other hand, the largest R_m and flux are gained in sample SF1, so in this sample, sieving separation has the least effect compared to other cases. However, sieving cannot be ignored due to the high flux, so all mechanisms had positive synergy in SF1. Each Fe_3O_4 has four oxygen, which can absorb and separate by four chemical bonds due to the activity of the sites. So chemical mechanism is superior to other mechanisms. As shown in Fig. 8, SF1 has a higher apparent roughness than other samples. However, its highest water content, which indicates its highest

Table 5: Comparison between prepared membrane's flux and rejection performance in this study and some reported ones

NPs	NPs W%	[a]Re_0	[b]$Flux_0$	[c]Re	[d]Flux	Re-Re_0/Re_0*100	Flux $Flux_0$/$Flux_0$*100	Ref
(a)Fe_3O_4	0.02	53.91	2.81	90.03	16.35	67.00	481.85	This study
(b)Fe_3O_4	0.1	82	3.2	84	4.3	2.44	34.38	[39]
(c)Fe_3O_4	0.5	61	11.5	59	9.5	-3.28	-17.39	[74]
(d)Fe_3O_4	1	53.5	0.9	60.78	2.01	13.61	123.33	[75]
(a)8-HQ/ Fe_3O_4	0.05	58.55	7.1	65	9.6	11.02	35.21	[76]
(b)8-HQ/ Fe_3O_4	0.2	58.55	7.1	96	21.5	63.96	202.82	[76]
(a)Fe_3O_4 treated with trisodium citrate	0.01	22	8.8	30.5	15.5	38.64	76.14	[22]
(b)Fe_3O_4 treated with trisodium citrate	1	22	8.8	36	21.3	63.64	142.05	[22]
(a)Fe_3O_4-PVP	0.05	82	3.2	87	6.5	6.10	103.13	[39]
(b)Fe_3O_4-PVP	0.1	82	3.2	90	6.45	9.76	101.56	[39]
(a)PAA- Fe_3O_4	0.05	53.5	2.68	90.5	1.6	69.16	-40.30	[75]
(b)PAA-Fe_3O_4	1	53.5	0.9	64.68	2.68	20.90	197.78	[75]
PVA/ Fe_3O_4 layer	4% coated	77	26	93	14	20.78	-46.15	[22]
sodium citrate surfactant/iron oxide	0.50	61.00	11.50	67.80	18.40	11.15	60.00	[74]

[a] Rejection performance of pure PES

[b] Pure water flux of pure PES

[c] Rejection performance of prepared membrane

[d] Pure water flux of prepared membranes

hydrophilicity, is due to the relative roughness effect of chemical bonds found in most mineral oxides [72, 73], confirming that the predominant mechanism is the chemical-magnetic mechanism in SF1. Because of agglomeration and increased effective size of NPs in SF2 and SF3 onwards, the chemical effect has decreased compared with SF1. In SF2, the mean pore sizes do not change much and the reductions observed in flux and separation can be attributed to the decrease in the Donnan mechanism. Because the dispersion of nanoparticles in SF2 is better than in SF3, the Donnan effect is more effective. There is no nanoparticle in SF0, and its pore size is larger, so the predominant separation in SF0 is the sieving mechanism.

SF1 has the highest thickness of the thin layer and the highest surface charge is seen in this membrane. Therefore, this membrane has the most rejection performance and water flux. In addition, chemical and sieving separation and electrostatic repulsion in this membrane are more than in other membranes. As the concentration of NPs increase, the phase change rate increases, so the thin layer thickness decreases, and the sieving separation decreases. With increasing agglomeration phenomenon and misalignment of spins, the surface charge of the membrane is reduced, so electrostatic separation is reduced. In SF2, the entrance of the channels is closed and the interchannels are blocked. As a result, it causes water retention in the blocked channels and reduces rejection performance and water flux. However, in SF3, because the agglomeration has moved slightly upwards due to the increase in the rate of phase change and sometimes transferred to the thin layer, the obstruction of the channels is less than in SF2 and a slight rise in flux can be observed.

All of the systems evaluated in this study are dead-end nanofiltration systems, and two nondimensional parameters define the performance of the base membrane. Table 5 and Fig. 14 compare the properties of the Fe_3O_4/PES membrane, including water flux and rejection performance, with those reported in other studies. The results show that the performance of the Fe_3O_4/PES membrane is comparable to the reported membranes and better in some cases. The table lists the water flux and rejection performance values reported in several articles. It is clear that the values obtained in the present study demonstrate better performance than other reports, with much less consumption of nanoparticles.

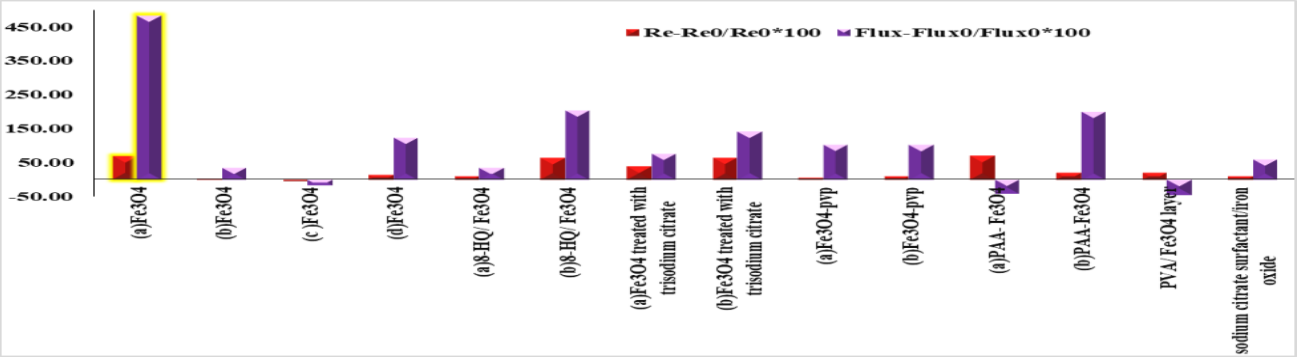

Fig. 14: Comparison between the flux and rejection performance of Fe_3O_4 /PES in this study and some reported ones

Moreover, the increase in flux is much less in these cases than in the present study. In general, this work is economically superior due to the low consumption of NPs. However, future investigations should identify optimal conditions to prevent NP accumulation. Creating a membrane with a higher magnetic strength may also be possible for specific purposes.

CONCLUSIONS

NF membranes based on PES were fabricated through phase inversion methods and different concentrations of Fe_3O_4 NPs were embedded in the membrane body. The effect of the incorporated Fe_3O_4 NPs on the morphological properties of the membrane was studied using FT-IR, XRD, SEM, and 3D surface images. The 3D images and EDX mapping indicated a relatively uniform distribution of NPs in the membrane matrix. In addition, the results revealed higher surface hydrophilicity and prominent flux for the Fe_3O_4 /PES compared to the neat membrane. On the other hand, flux was mainly improved by incorporating Fe_3O_4 NPs in the polymeric matrix. The maximum flux, 16.35 (L/m^2h), was obtained for PES-0.01 wt.% Fe_3O_4 in the membrane matrix, while 2.81 (L/m^2h) was observed for the bar membrane.

Moreover, the salt rejection increased from 60% for a virgin PES membrane to 90% for the modified membrane. The nanoparticle used is, at best, one-tenth of the nanoparticle used in similar works by other researchers. This indicates that this research is much more economical under similar operating conditions than in similar cases.

Acknowledgments

The authors gratefully acknowledge Iran National Science Foundation: INSF and Laboratory Network of Strategic Technologies of Iran (Labsnet) for providing financial support (Grant No. 99000876, Grants No.8344&8691, respectively) during the study. Additionally, genuinely thank Arak University for its financial and spiritual support.

Received : Jan. 19, 2023 ; Accepted : Apr.24, 2023

REFERENCES

[1] Miller D.J., Dreyer D.R., Bielawski C.W., Paul D.R., Freeman B.D., Surface Modification of Water Purification Membranes, *Angewandte Chemie International Edition*, **56**: 4662-4711 (2017).

[2] Tul Muntha S., Kausar A., Siddiq M., Advances in Polymeric Nanofiltration Membrane: A Review, *Polymer-Plastics Technology and Engineering*, **56**: 841-856 (2017).

[3] Heidari H., F Aliramezani., Ni /Fe_3O_4@Nanocellulose and Ni/Nanocellulose Green Nanocomposites: Inorganic- Organic Hybrid Catalysts for the Reduction of Organic Pollutants, *Iran. J. Chem. Chem. Eng. (IJCCE)*, **41(10):**3293-3303 (2022).

[4] Elizalde C.N.B., Al-Gharabli S., Kujawa J., Mavukkandy M., Hasan S.W., Arafat H.A., Fabrication of Blend Polyvinylidene Fluoride/Chitosan Membranes for Enhanced Flux and Fouling Resistance, *Separation and Purification Technology*, **190**: 68-76 (2018).

[5] Salehi M., Karimipour G., Montazerozohoori M., Ghaedi M., Mandanipour V., New Proton-Exchange Membrane (PEM) Based on the Modification of Sulfonated Polystyrene with MIL-53(Al)-NH_2 for Direct-Methanol Fuel Cell, *Iranian Journal of Chemistry and Chemical Engineering (IJCCE)*, **41(10):** 4117-4126 (2022).

[6] Zangeneh H., Zinatizadeh A.A., Zinadini S., Feyzi M., Bahnemann D.W., Preparation and Characterization of a Novel Photocatalytic Self-Cleaning PES Nanofiltration Membrane by Embedding a Visible-Driven Photocatalyst Boron Doped-$TiO_2SiO_2/CoFe_2O_4$ Nanoparticles, *Separation and Purification Technology*, **209**: 764-775 (2019).

[7] Daraei P., Madaeni S.S., Ghaemi N., Monfared H.A., Khadivi M.A., Fabrication of PES Nanofiltration Membrane by Simultaneous Use of Multi-Walled Carbon Nanotube and Surface Graft Polymerization Method: Comparison of MWCNT and PAA Modified MWCNT, *Separation and Purification Technology*, **104**: 32-44 (2013).

[8] Abdali N., Marjani A., Heidary F., Adimi M., Fabrication of PVA Coated PES/PVDF Nanocomposite Membranes Embedded with in Situ Formed Magnetite Nanoparticles for Removal of Metal Ions from Aqueous Solutions, *New Journal of Chemistry*, **41**: 6405-6414 (2017).

[9] Modabberasl A., Pirhoushyaran T., Esmaeili-Faraj S.H., Synthesis of $CoFe_2O_4$ Magnetic Nanoparticles for Application in Photocatalytic Removal of Azithromycin from Wastewater, *Scientific Reports*, **12**: 19171 (2022).

[10] Parvizi M.R., Saadati Z., Maleki A., Investigating the Performance of Nano Composite Membrane Pebax/TiO_2 Nanoparticle Modified with Amino Silane in the Separation of CO_2/CH_4, *Iran. J. Chem. Chem. Eng. (IJCCE)*, **42(3):**754-773 (2023).

[11] Muthuraman G., Tow Teng T., Simultaneous Extraction and Stripping of Methylene Blue: A Liquid-Liquid Extraction and Bulk Liquid Membrane Approach, *Iran. J. Chem. Chem. Eng. (IJCCE)*, **41(10):** 3451-3462 (2022).

[12] Gandomkar E., Bekhradinasab E., Sabbaghi S., Zerafat M.M., "Improvement of Chemical Demulsifier Performance Using Silica Nanoparticles", World Academy of Science, Engineering and Technology, (2015).

[13] Gandomkar E., Sabbaghi S., Investigation of the Morphology of SiO_2 Nanoparticles Using Different Synthesis Techniques *World Academy of Science, Engineering and Technology, International Journal of Chemical and Molecular Engineering*, **9(4)**: 2015 (2015).

[14] Fazlali A., Ghalehkhondabi V., Alahyarpur F., The Experimental Comparison between the Effect of Copper Oxide and Graphene Nanoparticles on Rheological Behavior and Thermal Properties of Engine Oil, *Petroleum Science and Technology*, **40**: 803-821 (2022).

[15] Abdekhodaie M.J., Hemmati A.A., Influence of Formulation Parameters on the Release of Diclofenac Sodium from Matrices with Manufacturing Formulation Ingredients, *Iranian Journal of Chemistry and Chemical Engineering (IJCCE)*, **21(2):** 135-140(2002).

[16] Mohamadpour M., Pirdashti M., Shahrokhi B., Rostami A.A., Response Surface Methodology for the Evaluation of Lysozyme Partitioning in Poly (Vinyl Pyrrolidone) and Potassium Phosphate Aqueous Two-Phase System, *Iranian Journal of Chemistry and Chemical Engineering (IJCCE)*, **38(5):** 197-208 (2019).

[17] Hosseini E.S., Pirdashti M., Influence of the Molecular Weight of Polymer on the Poly Vinyl Pyrrolidone and Zinc Sulfate Phase Diagram of Aqueous Two-Phase Systems, *Iranian Journal of Chemistry and Chemical Engineering (IJCCE)*, **40(2):** 627-637 (2021).

[18] Farahani F., Fazlali A., Kazazi M., Chemical Deposition of Nickel Hexacyanoferrate Nanoparticles on a Stainless-Steel Mesh Substrate for Supercapacitor Application, *Journal of Advanced Materials and Technologies*, **11**: 45-56(2022).

[19] Pandey G., Singh S., Hitkari G., Synthesis and Characterization of Polyvinyl Pyrrolidone (PVP)-Coated Fe_3O_4 Nanoparticles by Chemical Co-Precipitation Method and Removal of Congo Red dye by Adsorption Process, *International Nano Letters*, **8**: 111-121 (2018).

[20] Daraei P., Madaeni S.S., Ghaemi N., H. Ahmadi Monfared, Khadivi M.A., Fabrication of PES Nanofiltration Membrane by Simultaneous use of Multi-Walled Carbon Nanotube and Surface Graft Polymerization Method: Comparison of MWCNT and PAA Modified MWCNT, *Separation and Purification Technology*, **104**: 32-44(2013).

[21] Daraei P., Madaeni S.S., Ghaemi N., Khadivi M.A., Astinchap B., Moradian R., Fouling Resistant Mixed Matrix Polyethersulfone Membranes Blended with Magnetic Nanoparticles: Study of Magnetic Field Induced Casting, *Separation and Purification Technology*, **109**: 111-121 (2013).

[22] Ghaemi N., Madaeni S.S., P Daraei., H Rajabi., Zinadini S., Alizadeh A., Heydari R., Beygzadeh M., Ghouzivand S., Polyethersulfone Membrane Enhanced with Iron Oxide Nanoparticles for copper Removal from Water: Application of New Functionalized Fe3O4 Nanoparticles, *Chemical Engineering Journal*, **263**: (2015) 101-112.

[23] Aghaaliakbari B., Jafari Jaid A., Zeinali M.A.A., Computational Simulation of Ablation Phenomena in Glass-Filled Phenolic Composites, *Iranian Journal of Chemistry and Chemical Engineering (IJCCE)*, **34(1):** 97-106 (2015).

[24] Rahmanzadeh M., Rezakhani N., Zeinali Danalou S., Rostami F., Khosharay S., Cetyltrimethylammonium Bromide (CTAB), Additives and Their Mixtures: The Experimental and Modeling Study, *Iranian Journal of Chemistry and Chemical Engineering (IJCCE)*, **41(2):** 555-565 (2022).

[25] S Zinadini., Zinatizadeh A.A., M Rahimi., Vatanpour V., Zangeneh H., Preparation of a Novel Antifouling Mixed Matrix PES Membrane by Embedding Graphene Oxide Nanoplates, *Journal of Membrane Science*, **453**: 292-301(2014).

[26] Javaheri F., Hassanajili S., Synthesis of Fe_3O_4@SiO_2@MPS@P_4VP Nanoparticles for Nitrate Removal from Aqueous Solutions, *Journal of Applied Polymer Science*, **133**: (2016).

[27] Hebbar R.S., Isloor A.M., Ananda K., Abdullah M.S., Ismail A.F., Fabrication of a Novel Hollow Fiber Membrane Decorated with Functionalized Fe_2O_3 Nanoparticles: Towards Sustainable Water Treatment and Biofouling Control, *New Journal of Chemistry*, **41**: 4197-4211(2017).

[28] Esmaeili-Faraj S.H., Hassanzadeh A., Shakeriankhoo F., Hosseini S., Vaferi B., Diesel fuel Desulfurization by Alumina/Polymer Nanocomposite Membrane: Experimental Analysis and Modeling by the Response Surface Methodology, *Chemical Engineering and Processing - Process Intensification*, **164**: 108396 (2021).

[29] Alenazi N.A., M Hussein.A., Alamry K.A., Asiri A.M., Modified Polyether-Sulfone Membrane: A Mini Review, *Designed Monomers and Polymers*, **20**: 532-546 (2017).

[30] Azile N., Anele M., Richard M.M., Philiswa N.N., Wastewater Treatment Using Membrane Technology, in: Y. Taner (Ed.) "Wastewater and Water Quality", IntechOpen, Rijeka, Ch. 2., (2018).

[31] Barakat M., New Trends in Removing Heavy Metals from Industrial Wastewater, *Arabian Journal of Chemistry*, **4**: 361-377 (2011).

[32] G. E., "Removal Dye Pollutions & turbidity of inorganic & Organic Medium Using Nanostructures", In Chemical Engineering., Engineering, Shiraz University, Shiraz University, 2014.

[33] Wei Y., Han B., Hu X., Lin Y., Wang X., Deng X., Synthesis of Fe3O4 Nanoparticles and their Magnetic Properties, *Procedia Engineering*, **27** 632-637(2012).

[34] Prabhu Y.T., Rao K.V., Kumari B.S.,. Kumar V.S.S, Pavani T., Synthesis of Fe_3O_4 Nanoparticles and Its Antibacterial Application, *International Nano Letters*, **5**: 85-92 (2015).

[35] Wu W., He Q., Jiang C., Magnetic Iron Oxide Nanoparticles: Synthesis and Surface Functionalization Strategies, *Nanoscale Research Letters*, **3**: 397 (2008).

[36] Gohari B., Abu-Zahra N., Polyethersulfone Membranes Prepared with 3-Aminopropyltriethoxysilane Modified Alumina Nanoparticles for Cu(II) Removal from Water, *ACS Omega*, **3**: 10154-10162 (2018).

[37] Muharrem I., Olcay Kaplan I., Preparation and Applications of Nanocomposite Membranes for Water/Wastewater Treatment, in: I. Muharrem, I. Olcay Kaplan (Eds.) "Osmotically Driven Membrane Processes", IntechOpen, Rijeka, Ch. 1 (2022).

[38] Deboli F., Van der Bruggen B., Donten M.L., A Versatile Chemistry Platform for the Fabrication of Cost-Effective Hierarchical Cation and Anion Exchange Membranes, *Desalination*, **535**: 115794(2022).

[39] Fazlali A., Van der Bruggen B., Hosseini S., Afshari M., Farahani S.K., Bandehali S., Bagheripour E., Mixed Matrix PES-Based Nanofiltration Membrane Decorated by (Fe_3O_4–Polyvinylpyrrolidone) Composite Nanoparticles with Intensified Antifouling and Separation Characteristics, *Chemical Engineering Research and Design*, **147**: 390-398 (2019).

[40] Li J.F., Xu Z.L., Yang H., Feng C.P., Shi J.H., Hydrophilic Microporous PES Membranes Prepared by PES/PEG/DMAc Casting Solutions, *Journal of Applied Polymer Science*, **107**: 4100-4108 (2008).

[41] Zhang X., Jin P., Xu D., Zheng J., Zhan Z.-M., Gao Q., S Yuan., Z Xu.-L., Van der Bruggen B., Triethanolamine Modification Produces Ultra-Permeable Nanofiltration Membrane with Enhanced Removal Efficiency of Heavy Metal Ions, *Journal of Membrane Science*, **644**:120127(2022).

[42] Zheng J., R Zhao., Uliana A.A., Liu Y., de Donnea D., Zhang X., Xu D., Gao Q., Jin P., Y Liu., Volodine A., Zhu J., Van der Bruggen B., Separation of Textile Wastewater Using a Highly Permeable Resveratrol-Based Loose Nanofiltration Membrane with Excellent Anti-Fouling Performance, *Chemical Engineering Journal*, **434**: 134705 (2022).

[43] Zhang X., J Zheng., Jin P., Xu D., S Yuan., Zhao R., S Depuydt., Gao Y., Xu Z.-L., Van der Bruggen B., A PEI/TMC Membrane Modified with an Ionic Liquid with Enhanced Permeability and Antibacterial Properties for the Removal of Heavy Metal Ions, *Journal of Hazardous Materials*, **435**: 129010(2022).

[44] Liu J., Dai C., Hu Y., Aqueous Aggregation Behavior of Citric Acid Coated Magnetite Nanoparticles: Effects of pH, Cations, *Anions, And Humic Acid, Environmental Research*, **161**: 49-60 (2018).

[45] Singh D., Gautam R.K., R Kumar., Shukla B.K., Shankar V., V Krishna., Citric Acid Coated Magnetic Nanoparticles: Synthesis, Characterization and Application in Removal of Cd (II) Ions from Aqueous Solution, *Journal of Water Process Engineering*, **4**: 233-241 (2014).

[46] Lu X., Niu M., Qiao R., Gao M., Superdispersible PVP-Coated Fe3O4 Nanocrystals Prepared by a “one-Pot” Reaction, *The Journal of Physical Chemistry B*, **112**: 14390-14394 (2008).

[47] Khayet M., García-Payo M.d.C., X-Ray Diffraction Study of Polyethersulfone Polymer, Flat-Sheet and Hollow Fibers Prepared from the Same under Different Gas-Gaps, *Desalination*, **245**: (494-5002009).

[48] Barakat M.A., New Trends in Removing Heavy Metals from Industrial Wastewater, *Arabian Journal of Chemistry*, **4**: 361-377(2011).

[49] Baghbanzadeh M., Rana D., Matsuura T., Lan C.Q., Effects of Hydrophilic CuO Nanoparticles on Properties and Performance of PVDF VMD Membranes, *Desalination*, **369**: (2015) 75-84.

[50] Boughdiri A., Ounifi I., Chemingui H., Ursino C., Gordano A., Zouaghi M.O., A Hafiane., Figoli A., Ferjani E., A Preliminary Study on Cellulose Acetate Composite Membranes: Effect of Nanoparticles Types in their Preparation and Application, *Materials Research Express*, (2021).

[51] Yip N.Y., Tiraferri A., W. Phillip A., J Schiffman.D., Elimelech M., High Performance Thin-Film Composite Forward Osmosis Membrane, *Environmental Science & Technology*, **44**: 3812-3818 (2010).

[52] P.S. Goh, A.F. Ismail, "Chapter 5 - Flat-Sheet Membrane for Power Generation and Desalination Based on Salinity Gradient, in: S. Sarp, N. Hilal (eds.) Membrane-Based Salinity Gradient Processes for Water Treatment and Power Generation", Elsevier,155-174 (2018).

[53] Touati K., Tadeo F., Chapter One - Pressure Retarded Osmosis as Renewable Energy Source, in: Touati K., Tadeo F., Chae S.H., Kim J.H., Alvarez-Silva O. (eds.) “Pressure Retarded Osmosis", *Academic Press*, 1-54 (2017).

[54] Rashid K.T., Alayan H.M., Mahdi A.E., Al-Baiati M.N., Majdi H.S., Salih I.K., Ali J.M., Alsalhy Q.F., Novel Water-Soluble Poly(terephthalic-Co-Glycerol-g-Fumaric Acid) Copolymer Nanoparticles Harnessed as Pore Formers for Polyethersulfone Membrane Modification: Permeability– Selectivity Tradeoff Manipulation, *Water*, **14**: (2022).

[55] Huang Z.-H., Zhang X., Wang Y.-X., Sun J.-Y., Zhang H., Liu W.-L., Li M.-P., Ma X.-H., Xu Z.-L., Fe3O4/PVDF Catalytic Membrane Treatment Organic Wastewater with Simultaneously Improved Permeability, Catalytic Property and Anti-Fouling, *Environmental Research*, **187**: 109617 (2020).

[56] Zare S., Kargari A., 4 - Membrane Properties in Membrane Distillation, in: V.G. Gude (Ed.) Emerging Technologies for Sustainable Desalination Handbook, *Butterworth-Heinemann*, 107-156 (2018).

[57] Greenlee L.F., N Rentz.S., Influence of Nanoparticle Processing and Additives on PES Casting Solution Viscosity and cast Membrane Characteristics, *Polymer*, **103**: 498-508 (2016).

[58] Zhang Z., An Q., Ji Y., Qian J., Gao C., Effect of Zero Shear Viscosity of the Casting Solution on the Morphology and Permeability of Polysulfone Membrane Prepared via the Phase-Inversion Process, *Desalination*, **260**: 43-50 (2010).

[59] Hołda A.K., Vankelecom I.F.J., Understanding and Guiding the Phase Inversion Process for Synthesis of Solvent Resistant Nanofiltration Membranes, *Journal of Applied Polymer Science*, **132**: (2015) n/a-n/a.

[60] Bahramian A., Danesh A., Prediction of Solid–Fluid Interfacial Tension and Contact Angle, *Journal of Colloid and Interface Science*, **279**: 206-212 (2004).

[61] Long J., Hyder M., Huang R., Chen P., Thermodynamic Modeling of Contact Angles on Rough, Heterogeneous Surfaces, *Advances in Colloid and Interface Science*, **118**: 173-190 (2005)

[62] Lv C., Su Y., Wang Y., Ma X., Sun Q., Jiang Z., Enhanced Permeation Performance of Cellulose Acetate Ultrafiltration Membrane by Incorporation of Pluronic F127, *Journal of Membrane Science*, **294**: 68-74 (2007).

[63] Yu H., Zhang Y., X Sun., Liu J., Zhang H., Improving the Antifouling Property of Polyethersulfone Ultrafiltration Membrane by Incorporation of Dextran Grafted Halloysite Nanotubes, *Chemical Engineering Journal*, **237**: 322-328 (2014)

[64] Huang F., Wang Q., Wei Q., Gao W., Shou H., Jiang S., Dynamic Wettability and Contact Angles of Poly (Vinylidene Fluoride) Nanofiber Membranes Grafted with Acrylic Acid, *Express Polymer Letters*, **4**: (2010).

[65] C Kee.M., Idris A., Modification of Cellulose Acetate Membrane Using Monosodium Glutamate Additives Prepared by Microwave Heating, *Journal of Industrial and Engineering Chemistry*, **18**: 2115-2123(2012).

[66] Zhao Y.-H., Zhu B.-K., Ma X.-T., Xu Y.-Y., Porous Membranes Modified by Hyperbranched Polymers: I. Preparation and Characterization of PVDF Membrane Using Hyperbranched Polyglycerol as Additive, *Journal of Membrane Science*, **290**: 222-229 (2007).

[67] Chan M., Ng S., Effect of Membrane Properties on Contact Angle, *AIP Conference Proceedings, AIP Publishing LLC*, , **2016(1)**: 020035 (2018).

[68] Vatanpour V., Madaeni S.S., Moradian R., S Zinadini., Astinchap B., Fabrication and Characterization of Novel Antifouling Nanofiltration Membrane Prepared from Oxidized Multiwalled Carbon Nanotube/Polyethersulfone Nanocomposite, *Journal of Membrane Science*, **375**: 284-294 (2011).

[69] Hegab H.M., Zou L., Graphene Oxide-Assisted Membranes: Fabrication and Potential Applications in Desalination and Water Purification, *Journal of Membrane Science*, **484**: 95-106 (2015).

[70] Wei X., Xu X., Wu J., Li C., Chen J., Lv B., Zhu B., Xiang H., SiO_2-Modified Nanocomposite Nanofiltration Membranes with High Flux and Acid Resistance, *Journal of Applied Polymer Science*, **136**: 47436 (2019).

[71] Al-Rashdi B., Johnson D., Hilal N., Removal of Heavy Metal Ions by Nanofiltration, *Desalination*, **315**: 2-17 (2013).

[72] Wolansky G., Marmur A., Apparent Contact Angles on Rough Surfaces: The Wenzel Equation Revisited, *Colloids and Surfaces A: Physicochemical and Engineering Aspects*, **156**: 381-388 (1999).

[73] Drelich J.W., Contact Angles: From Past Mistakes to New Developments through Liquid-Solid Adhesion Measurements, *Advances in Colloid and Interface Science*, **267**: 1-14 (2019).

[74] Moghadassi A., Moradi S., Bandehali S., Fabrication of Antifouling Mixed Matrix NF Membranes by Embedding Sodium Citrate Surfactant Modified-Iron Oxide Nanoparticles, *Korean Journal of Chemical Engineering*, **37**: 1963-1974 (2020).

[75] Bagheripour E., Moghadassi A., Hosseini S.M., Incorporated Poly Acrylic Acid-Co-fe3o4 Nanoparticles Mixed Matrix Polyethersulfone Based Nanofiltration Membrane in Desalination Process, *International Journal of Engineering*, **30** 821-829 (2017).

[76] Ansari S., Moghadassi A., Hosseini S.M., A New Approach to Tailoring the Separation Characteristics of Polyethersulfone Nanofiltration Membranes by 8-Hydroxyquinoline Functionalized Fe_3O_4 Nanoparticles, *Korean Journal of Chemical Engineering*, **37**: 2011-2019 (2020).